Orthogonal precoding with memory for sidelobe suppression in OFDM

Khawar Hussain Roberto López-Valcarce
atlanTTic Research Center, Universidade de Vigo, Spain
{khawar,valcarce}@gts.uvigo.es

***Abstract*—Orthogonal precoding is a very effective approach to reduce out-of-band radiation (OBR) in multicarrier systems in order to avoid adjacent channel interference. This is achieved at the cost of introducing precoder redundancy, which results in throughput loss. Introducing memory in the precoding operation has the potential to improve performance without sacrificing additional spectral efficiency, in exchange for extra computational complexity. We present a novel orthogonal memory precoder which minimizes OBR within a user-selectable frequency region and allows for controlling spectral overshoot. Decision-feedback decoding avoids symbol error rate degradation at the receiver.**

***Index Terms*—OFDM, out-of-band radiation, sidelobe suppression, spectral precoding, orthogonal precoding.**

I. Introduction

The fifth-Generation New Radio (5G-NR) interface has adopted cyclic-prefix (CP) based orthogonal frequency division multiplexing (OFDM) as waveform [1]. OFDM is a mature technology with significant advantages: it is spectrally efficient, robust against multipath effects, and well matched to multiple input-multiple output (MIMO) operation. However, it suffers from large spectrum sidelobes, causing high out-of-band radiation (OBR) and adjacent channel interference. Traditional techniques to address this issue, including guard band insertion, filtering [2], or windowing (pulse shaping) [3]–[5], are straightforward, but they either reduce the effective CP length or degrade spectral efficiency.

Another approach to OBR reduction is spectral precoding [6]–[10], in which the transmitted samples are obtained by some transformation of the original data sequence. Since this introduces distortion, some appropriate decoding may be required at the receiver side to avoid symbol error rate (SER) degradation. In orthogonal precoding, the precoder matrix is semi-unitary, i.e., with orthonormal columns; due to this property, the receiver can easily invert the precoding operation, avoiding noise enhancement and hence SER degradation. The OBR reduction is achieved at the cost of spectral efficiency: the number of data symbols per block modulated onto K available subcarriers is $K - R$, where $R \geq 0$ can be thought of as the redundancy of the precoder.

Most spectral precoding techniques modulate the subcarriers with a linear combination of the data values of the current OFDM symbol; hence, it is pertinent to ask whether spectral precoder performance could be improved by introducing memory, so that the data from OFDM symbols other than the current one enter the linear combination. We explored this idea in [11] for a particular class of spectral precoding, namely active interference cancellation (AIC), in which only a subset of R reserved subcarriers are precoded, whereas the $K - R$ data subcarriers remain undistorted. AIC is well suited to systems in which complexity at the receiver must be kept at a minimum (it only needs to discard samples received in reserved subcarriers), but its sidelobe suppression is limited.

The family of so-called N-continuous precoders [12]–[15], which impose continuity on the time-domain signal and several of its derivatives to reduce sidelobes, constitute a class of memory precoders in which a first-order infinite impulse response (IIR) filter is applied to the data sequence. This approach, however, is not flexible in the sense that it does not allow to select the frequency range of interest, or to adjust the level of spectral overshoot within the passband. Here we present a novel memory-based extension of orthogonal precoders resulting in finite impulse response (FIR) filtering of the data sequence, with filter coefficients designed to minimize OBR over a selectable frequency region, and with controllable spectral overshoot. A decision-feedback decoder effectively avoids SER degradation at the receiver. Simulation results show how the introduction of memory in the precoding operation helps improve the tradeoff between sidelobe suppression and spectral efficiency, at the cost of extra computational resources at the transmitter and receiver.

II. Signal Model

Consider an OFDM system with IFFT size N and CP of $N_{\rm cp}$ samples. A total of $K \leq N$ active subcarriers with indices $\mathcal{K} = \{k_1, k_2, \cdots k_K\}$ are available for transmission, and $x_k^{(m)} \in \mathbb{C}$ is the sample modulating the k-th subcarrier of the m-th symbol. With $L = N + N_{\rm cp}$ the symbol length, the baseband samples of the multicarrier signal are given by

$$s[n] = \sum_{m=-\infty}^{\infty} \sum_{k \in \mathcal{K}} x_k^{(m)} h_{\rm P}[n - mL] e^{j\frac{2\pi}{N}k(n-mL)}, \quad (1)$$

where $h_{\rm P}[n] \leftrightarrow H_{\rm P}(e^{j\omega})$ is the shaping pulse. The analog baseband signal is given by

$$s(t) = \sum_{n=-\infty}^{\infty} s[n] h_{\rm I}(t - nT_s), \quad (2)$$

with T_s being the sampling interval, and $h_{\rm I}(t) \leftrightarrow H_{\rm I}(f)$ the interpolation filter in the Digital-to-Analog Converter (DAC).

This work was funded by MCIN/ AEI/10.13039/501100011033/ FEDER "Una manera de hacer Europa" under project RODIN (PID2019-105717RB-C21) and fellowship BES-2017-080305.

The subcarrier spacing is thus $\Delta f = \frac{1}{NT_s}$. Let us define $\phi_k(f) \triangleq H_{\rm P}^*(e^{j2\pi(f-k\Delta f)T_s})$, and group these in the vector

$$\boldsymbol{\phi}(f) \triangleq \left[\begin{array}{cccc} \phi_{k_1}(f) & \phi_{k_2}(f) & \cdots & \phi_{k_K}(f) \end{array}\right]^T \in \mathbb{C}^K. \quad (3)$$

Let us collect the m-th block samples in the vector

$$\boldsymbol{x}_m \triangleq \left[\begin{array}{cccc} x_{k_1}^{(m)} & x_{k_2}^{(m)} & \cdots & x_{k_K}^{(m)} \end{array}\right]^T \in \mathbb{C}^K. \quad (4)$$

The power spectral density (PSD) of $s(t)$ is given by

$$S_s(f) = \frac{|H_{\rm I}(f)|^2}{LT_s} \boldsymbol{\phi}^H(f) \boldsymbol{S}_x(Lf) \boldsymbol{\phi}(f), \quad (5)$$

where $\boldsymbol{S}_x(f) = \sum_\ell \mathbb{E}\{\boldsymbol{x}_m \boldsymbol{x}_{m-\ell}^H\} e^{-j2\pi f T_s \ell}$, assuming that the process $\{\boldsymbol{x}_m\}$ is zero-mean and wide-sense stationary [16].

A. Spectral precoding

Let $\boldsymbol{d}_m \in \mathbb{C}^D$ be the vector of QAM-data for the m-th OFDM symbol, with $D \le K$ (thus, $R = K - D$ is the precoder redundancy). The sequence $\boldsymbol{x}_m \in \mathbb{C}^K$ is generated from $\boldsymbol{d}_m \in \mathbb{C}^D$ by means of a linear time-invariant precoder:

$$\boldsymbol{x}_m = \sum_\ell \boldsymbol{G}_\ell \boldsymbol{d}_{m-\ell}. \quad (6)$$

The standard memoryless architecture is obtained if $\boldsymbol{G}_\ell = \boldsymbol{0}$ for $\ell \neq 0$ in (6). Assuming $\mathbb{E}\{\boldsymbol{d}_m\} = \boldsymbol{0}$ and $\mathbb{E}\{\boldsymbol{d}_m \boldsymbol{d}_{m-\ell}^H\} = \delta_\ell \boldsymbol{I}_D$, then $\boldsymbol{S}_x(f) = \boldsymbol{G}(f)\boldsymbol{G}^H(f)$, where

$$\boldsymbol{G}(f) \triangleq \sum_\ell \boldsymbol{G}_\ell e^{-j2\pi f T_s \ell} \quad (7)$$

is the precoder transfer function. Hence, (5) becomes

$$S_s(f) = \frac{|H_{\rm I}(f)|^2}{LT_s} \left\| \boldsymbol{G}^H(Lf)\boldsymbol{\phi}(f) \right\|^2. \quad (8)$$

Let $W(f) \ge 0$ be a weighting function, and let $\widetilde{W}(f) \triangleq W(f)\frac{|H_{\rm I}(f)|^2}{LT_s}$. Then, the weighted power of $s(t)$ is

$$\begin{aligned} P_W &= \int_{-\infty}^{\infty} W(f) S_s(f) df \\ &= \mathrm{tr} \int_{-\infty}^{\infty} \widetilde{W}(f) \boldsymbol{G}^H(Lf)\boldsymbol{\phi}(f)\boldsymbol{\phi}^H(f)\boldsymbol{G}(Lf) df \\ &= \mathrm{tr} \sum_\ell \sum_{\ell'} \boldsymbol{G}_{\ell'}^H \boldsymbol{\Phi}[\ell - \ell'] \boldsymbol{G}_\ell, \end{aligned} \quad (9)$$

where we have introduced the $K \times K$ matrices

$$\boldsymbol{\Phi}[b] \triangleq \int_{-\infty}^{\infty} \widetilde{W}(f)\boldsymbol{\phi}(f)\boldsymbol{\phi}^H(f) e^{-j2\pi L f T_s b} df. \quad (10)$$

Thus, (9) gives the weighted power P_W in terms of of the precoder impulse response $\boldsymbol{G}_\ell$. More explicitly, and assuming a causal FIR precoder of order ℓ_0, let us introduce the matrices

$$\boldsymbol{G} \triangleq \left[\begin{array}{cccc} \boldsymbol{G}_0^H & \boldsymbol{G}_1^H & \cdots & \boldsymbol{G}_{\ell_0}^H \end{array}\right]^H, \quad (11)$$

$$\boldsymbol{\Phi} \triangleq \left[\begin{array}{cccc} \boldsymbol{\Phi}[0] & \boldsymbol{\Phi}[1] & \cdots & \boldsymbol{\Phi}[\ell_0] \\ \boldsymbol{\Phi}^H[1] & \boldsymbol{\Phi}[0] & \cdots & \boldsymbol{\Phi}[\ell_0 - 1] \\ \vdots & \vdots & \ddots & \vdots \\ \boldsymbol{\Phi}^H[\ell_0] & \boldsymbol{\Phi}^H[\ell_0 - 1] & \cdots & \boldsymbol{\Phi}[0] \end{array}\right]. \quad (12)$$

Note that $\boldsymbol{\Phi}$ is Hermitian block-Toeplitz. Then (9) becomes

$$P_W = \mathrm{tr}\left\{\boldsymbol{G}^H \boldsymbol{\Phi} \boldsymbol{G}\right\}. \quad (13)$$

B. Decoder

We constrain $\boldsymbol{G}_0$ to have orthonormal columns, which allows the following DF strategy for decoding. Let $\boldsymbol{r}_m$ be the vector at the receiver after FFT, CP removal, and frequency-domain equalization; then $\boldsymbol{r}_m = \sum_{\ell=0}^{\ell_0} \boldsymbol{G}_\ell \boldsymbol{d}_{m-\ell} + \boldsymbol{w}_m$, where $\boldsymbol{w}_m$ is the noise vector. The estimate of $\boldsymbol{d}_m$ is obtained as

$$\hat{\boldsymbol{d}}_m = \mathrm{DEC}\left\{ \boldsymbol{G}_0^H \left(\boldsymbol{r}_m - \sum_{\ell=1}^{\ell_0} \boldsymbol{G}_\ell \hat{\boldsymbol{d}}_{m-\ell} \right) \right\}, \quad (14)$$

where $\mathrm{DEC}\{\cdot\}$ is an entrywise hard-decision operator, returning for each entry its closest point in the constellation. In the absence of error propagation, $\hat{\boldsymbol{d}}_{m-\ell} \approx \boldsymbol{d}_{m-\ell}$ for $1 \le \ell \le \ell_0$, so that $\boldsymbol{r}_m - \sum_{\ell=1}^{\ell_0} \boldsymbol{G}_\ell \hat{\boldsymbol{d}}_{m-\ell} \approx \boldsymbol{G}_0 \boldsymbol{d}_m + \boldsymbol{w}_m$, and since $\boldsymbol{G}_0^H \boldsymbol{G}_0 = \boldsymbol{I}_D$, the decision variable in (14) becomes

$$\boldsymbol{G}_0^H \left(\boldsymbol{r}_m - \sum_{\ell=1}^{\ell_0} \boldsymbol{G}_\ell \hat{\boldsymbol{d}}_{m-\ell} \right) \approx \boldsymbol{d}_m + \widetilde{\boldsymbol{w}}_m, \quad (15)$$

where $\widetilde{\boldsymbol{w}}_m = \boldsymbol{G}_0^H \boldsymbol{w}_m$. Since $\mathbb{E}\{\|\widetilde{\boldsymbol{w}}_m\|^2\} \le \mathbb{E}\{\|\boldsymbol{w}_m\|^2\}$, see, e.g. [17], the DF decoder avoids noise enhancement.

III. Proposed Precoder Design

The goal is to minimize OBR over some region $\mathcal{B}$. We define OBR as (9), with $W(f) = 0$ outside $\mathcal{B}$, whereas $W(f) \ge 0$ for $f \in \mathcal{B}$ allows to emphasize OBR reduction over certain subbands. Note that $\mathcal{B}$ may include frequencies within the passband, e.g., to protect narrowband transmissions from other users in a dynamic spectrum sharing (DSS) setting. Let $P_T = \int_\infty^\infty S_s(f) df$ be the total transmit power, and let $P_{\rm ref}$ be the reference transmit power of an unprecoded system in which $\boldsymbol{x}_m = \boldsymbol{S}\boldsymbol{d}_m$, with $\boldsymbol{S}$ comprising the columns of $\boldsymbol{I}_K$ with indices given by the positions of the D active subcarriers. Defining $\boldsymbol{\Phi}_T[b]$ and $\boldsymbol{\Phi}_T$ analogously to (10) and (12) respectively, but for $W(f) = 1\ \forall f$, one has $P_T = \mathrm{tr}\{\boldsymbol{G}^H \boldsymbol{\Phi}_T \boldsymbol{G}\}$ and $P_{\rm ref} = \mathrm{tr}\{\boldsymbol{S}^H \boldsymbol{\Phi}_T[0] \boldsymbol{S}\}$. The problem can be stated as

$$\min_{\boldsymbol{G}} P_W \quad \text{s.to} \quad \left\{ \begin{array}{rcl} P_T & \le & \beta P_{\rm ref}, \\ \boldsymbol{G}_0^H \boldsymbol{G}_0 & = & \boldsymbol{I}_D, \end{array} \right. \quad (16)$$

where the scaling factor $\beta > 0$ is used to control the spectral peak by setting the maximum transmit power $\beta P_{\rm ref}$. Letting $\widetilde{\boldsymbol{G}} = [\boldsymbol{G}_1^H\ \boldsymbol{G}_2^H\ \cdots\ \boldsymbol{G}_{\ell_0}^H]^H$, problem (16) becomes

$$\min_{\boldsymbol{G}_0, \widetilde{\boldsymbol{G}}} \mathrm{tr}\{\boldsymbol{G}^H \boldsymbol{\Phi} \boldsymbol{G}\} \quad \text{s.to} \quad \left\{ \begin{array}{rcl} \mathrm{tr}\{\boldsymbol{G}^H \boldsymbol{\Phi}_T \boldsymbol{G}\} & \le & \beta P_{\rm ref}, \\ \boldsymbol{G}_0^H \boldsymbol{G}_0 & = & \boldsymbol{I}_D. \end{array} \right. \quad (17)$$

This problem is not convex due to the orthonormality constraint on $\boldsymbol{G}_0$. Note that $\widetilde{\boldsymbol{G}}$ is only affected by the first constraint in (17); thus, for $\boldsymbol{G}_0$ given, $\widetilde{\boldsymbol{G}}$ is the solution to

$$\min_{\widetilde{\boldsymbol{G}}} \mathrm{tr}\{\boldsymbol{G}^H \boldsymbol{\Phi} \boldsymbol{G}\} \ \text{ s. to } \ \mathrm{tr}\{\boldsymbol{G}^H \boldsymbol{\Phi}_T \boldsymbol{G}\} \le \beta P_{\rm ref}. \quad (18)$$

Let $c = \mathrm{tr}\{\boldsymbol{G}_0^H \boldsymbol{\Phi}[0] \boldsymbol{G}_0\}$, and define the submatrices

$$\boldsymbol{Y} = \boldsymbol{\Phi}_{K+1:(\ell_0+1)K\ ,\ K+1:(\ell_0+1)K} \quad (19)$$

$$\boldsymbol{Z} = \boldsymbol{\Phi}_{K+1:(\ell_0+1)K\ ,\ 1:K} \quad (20)$$

with c_T, $\boldsymbol{Y}_T$, $\boldsymbol{Z}_T$ analogously defined in terms of $\boldsymbol{\Phi}_T$. Then (18) becomes

$$\begin{aligned} \min_{\widetilde{\boldsymbol{G}}} \quad & \mathrm{tr}\{\widetilde{\boldsymbol{G}}^H \boldsymbol{Y} \widetilde{\boldsymbol{G}}\} + 2\,\mathrm{Re}\,\mathrm{tr}\{\widetilde{\boldsymbol{G}}^H \boldsymbol{Z} \boldsymbol{G}_0\} + c \\ \text{s. to} \quad & \mathrm{tr}\{\widetilde{\boldsymbol{G}}^H \boldsymbol{Y}_T \widetilde{\boldsymbol{G}}\} + 2\,\mathrm{Re}\,\mathrm{tr}\{\widetilde{\boldsymbol{G}}^H \boldsymbol{Z}_T \boldsymbol{G}_0\} \\ & + c_T \;\le\; \beta P_{\text{ref}}, \end{aligned} \tag{21}$$

i.e., a Least Squares problem with a Quadratic Inequality constraint (LSQI). Following [18], its solution has the form

$$\widetilde{\boldsymbol{G}} = -\boldsymbol{M}_\lambda \boldsymbol{G}_0, \tag{22}$$

$$\boldsymbol{M}_\lambda = (\boldsymbol{Y} + \lambda \boldsymbol{Y}_T)^{-1} (\boldsymbol{Z} + \lambda \boldsymbol{Z}_T), \tag{23}$$

where λ is the Lagrange multiplier. Now, with $\boldsymbol{M}_\lambda$ as in (23), let us introduce the $K \times K$ matrices

$$\boldsymbol{A}_\lambda = \boldsymbol{\Phi}[0] - \boldsymbol{Z}^H \boldsymbol{M}_\lambda - \boldsymbol{M}_\lambda^H \boldsymbol{Z} + \boldsymbol{M}_\lambda^H \boldsymbol{Y} \boldsymbol{M}_\lambda, \tag{24}$$

$$\boldsymbol{B}_\lambda = \boldsymbol{\Phi}_T[0] - \boldsymbol{Z}_T^H \boldsymbol{M}_\lambda - \boldsymbol{M}_\lambda^H \boldsymbol{Z}_T + \boldsymbol{M}_\lambda^H \boldsymbol{Y}_T \boldsymbol{M}_\lambda. \tag{25}$$

Then the optimization problem (17) can be rewritten as

$$\min_{\boldsymbol{G}_0, \lambda} \mathrm{tr}\{\boldsymbol{G}_0^H \boldsymbol{A}_\lambda \boldsymbol{G}_0\} \;\text{ s. to }\; \begin{cases} \mathrm{tr}\{\boldsymbol{G}_0^H \boldsymbol{B}_\lambda \boldsymbol{G}_0\} \le \beta P_{\text{ref}}, \\ \boldsymbol{G}_0^H \boldsymbol{G}_0 = \boldsymbol{I}_D. \end{cases} \tag{26}$$

Finding the exact solution to (26) is challenging; instead, we obtain an approximate solution as follows. First, we neglect the presence of $\boldsymbol{G}_0$ in the first constraint in (26) and consider

$$\min_{\boldsymbol{G}_0} \mathrm{tr}\{\boldsymbol{G}_0^H \boldsymbol{A}_\lambda \boldsymbol{G}_0\} \;\text{ s. to }\; \boldsymbol{G}_0^H \boldsymbol{G}_0 = \boldsymbol{I}_D, \tag{27}$$

whose solution $\boldsymbol{G}_{0,\lambda}$ comprises the D least dominant eigenvectors of $\boldsymbol{A}_\lambda$. If $\boldsymbol{G}_{0,\lambda}$ does not satisfy the power constraint in (26), then it remains to determine the Lagrange multiplier λ. This can be done by imposing the transmit power constraint; thus, one must solve

$$\mathrm{tr}\{\boldsymbol{G}_{0,\lambda}^H \boldsymbol{B}_\lambda \boldsymbol{G}_{0,\lambda}\} = \beta P_{\text{ref}}, \tag{28}$$

involving a one-dimensional search over the scalar parameter λ. Although we lack formal proof, we conjecture that the left-hand side of (28) is monotonically decreasing in λ, so (28) can be efficiently solved using the bisection method.

IV. Complexity Analysis

The computation of the precoder described in Sec. III can be performed offline. At each step of the bisection method to solve (28), the matrices $\boldsymbol{M}_\lambda$, $\boldsymbol{A}_\lambda$ and $\boldsymbol{B}_\lambda$ must be obtained, followed by an eigenvalue decomposition (EVD) of $\boldsymbol{A}_\lambda$. Complexity is dominated by the matrix inversion required to obtain $\boldsymbol{M}_\lambda$, which is $\mathcal{O}(\ell_0^3 K^3)$ per iteration.

Regarding online complexity, for each OFDM symbol $\boldsymbol{d}_m$ the transmitter needs to compute $\boldsymbol{x}_m = \boldsymbol{G}_0 \boldsymbol{d}_m + \boldsymbol{G}_1 \boldsymbol{d}_{m-1} + \cdots + \boldsymbol{G}_{\ell_0} \boldsymbol{d}_{m-\ell_0}$. Since $\boldsymbol{G}_0$ has orthonormal columns, the product $\boldsymbol{G}_0 \boldsymbol{d}_m$ can be obtained with complexity $\mathcal{O}(K^2 - D^2)$ by using block reflectors [19]. For $\ell = 1, \ldots, \ell_0$, each of the products $\boldsymbol{G}_\ell \boldsymbol{d}_{m-\ell}$ requires in principle $\mathcal{O}(KD)$ operations. However, the matrices $\boldsymbol{G}_1, \ldots, \boldsymbol{G}_{\ell_0}$ resulting from the proposed design usually exhibit a significant number of small singular values, suggesting that they can be replaced by their best low-rank approximations with very small performance loss. If the corresponding ranks are $r_1, \ldots, r_{\ell_0}$, then the computation of $\boldsymbol{x}_m$ is $\mathcal{O}((K+D)(K-D+r))$, where $r = r_1 + \cdots + r_{\ell_0}$. At the receiver side, the decoder (14) has to be implemented for each OFDM symbol; it is readily checked that the corresponding complexity is the same as that at the transmitter, i.e., $\mathcal{O}((K+D)(K-D+r))$.

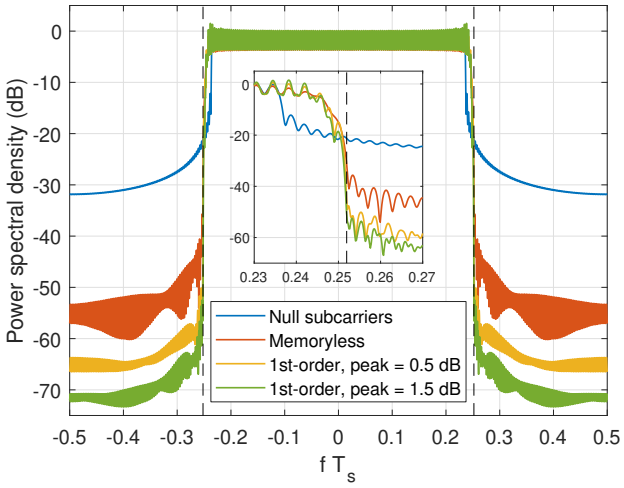

Fig. 1. PSDs of different precoder designs. $N = 256$, $N_{\text{cp}} = N/4$, $K = 129$, $R = 8$.

V. Numerical Examples

Consider a CP-OFDM setting with IFFT size $N = 256$ and $N_{\text{cp}} = N/4$. A rectangular pulse is adopted, i.e., $h_{\text{P}}[n] = 1$ for $0 \le n \le L-1$, and zero otherwise. The interpolation filter is an ideal lowpass filter: $H_{\text{I}}(f) = 1$ for $|f| \le \frac{1}{2T_s}$ and zero otherwise. A total of $K = 129$ active subcarriers are used and located symmetrically about the carrier frequency. The OBR region is $\mathcal{B} = \left\{ \frac{0.25}{T_s} + \frac{\Delta f}{2} \le |f| \le \frac{1}{2T_s} \right\}$. We consider a flat weighting function $W(f) = 1$ for $f \in \mathcal{B}$, and zero otherwise. As benchmarks, we consider (i) an unprecoded system with $R/2$ null subcarriers at each edge of the passband; (ii) the memoryless ($\ell_0 = 0$) orthogonal design [8], [9], in which $\boldsymbol{G}_0$ comprises the D least dominant eigenvectors of $\boldsymbol{\Phi}[0]$.

A. OBR vs. spectral peak

The value of β controls the maximum transmit power. Better OBR performance is achieved with larger β, at the cost of larger undesirable spectral peaks within the passband. Hence, an OBR/spectral overshoot tradeoff must be found by selecting β. To illustrate this, consider the application of the memoryless ($\ell_0 = 0$) and first-order ($\ell_0 = 1$) precoders with redundancy $R = 8$ in the setting described above. Fig. 1 shows the corresponding PSD curves. The total OBR (13) of the memoryless precoder is 21.4 dB below that of the unprecoded scheme with null subcarriers; for the 1st-order precoder with spectral peak of 0.5 and 1.5 dB, the corresponding figures are 32.9 and 38.2 dB, respectively. This tradeoff is further illustrated in Fig. 2, which shows the relative OBR as a

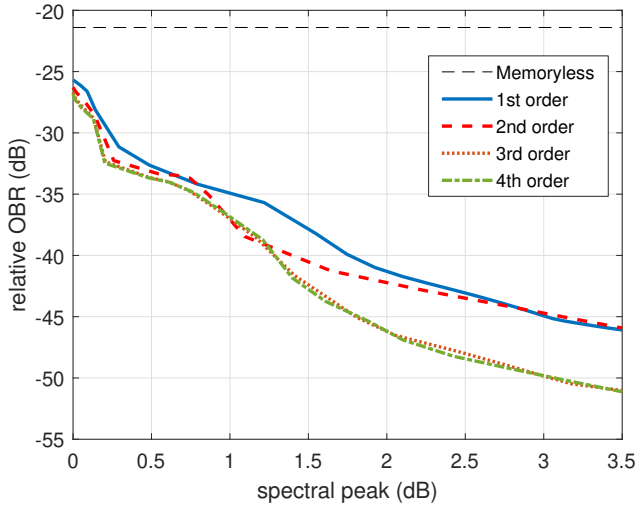

Fig. 2. OBR (relative to that of the unprecoded system) as a function of spectral peak. $N = 256$, $N_{\rm cp} = N/4$, $K = 129$, $R = 8$.

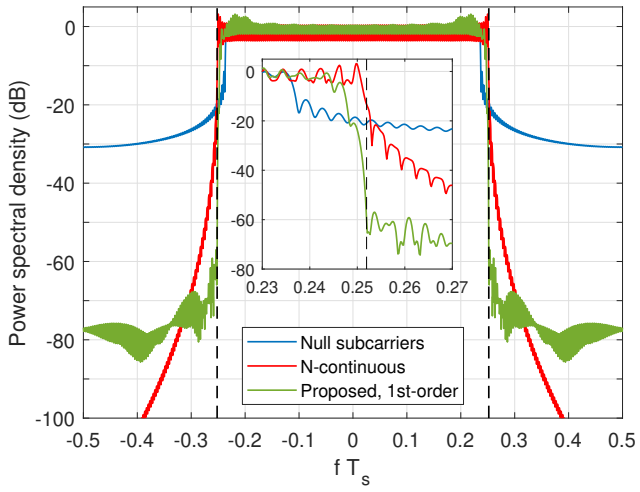

Fig. 3. PSDs of different designs. $N = 256$, $N_{\rm cp} = N/4$, $K = 129$, $R = 8$. Spectral peak is 3.2 dB for N-continuous and proposed precoders.

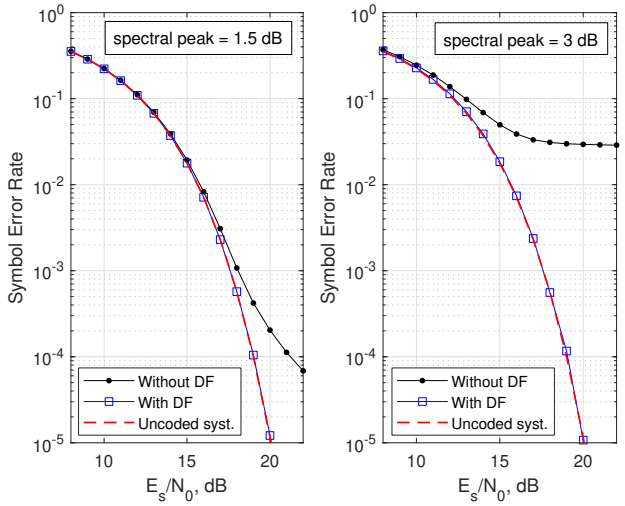

Fig. 4. SER of 1st-order memory precoder for 16-QAM in AWGN channel. $N = 256$, $N_{\rm cp} = N/4$, $K = 129$, $R = 8$.

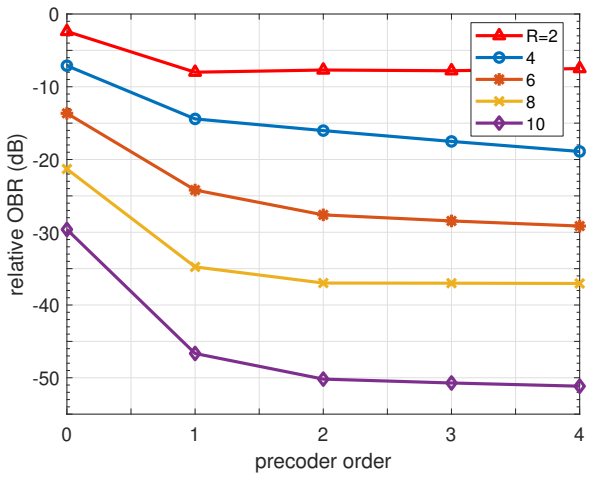

Fig. 5. OBR (relative to that of the unprecoded system) of the proposed design, for different values of order ℓ_0 and redundancy R. Spectral peak is set to 1 dB in all cases.

function of the spectral peak[1], for memory precoders up to 4th order. For the same parameter values of this setting, the N-continuous precoder from [14] yields a relative OBR of only -8.8 dB, with a spectral peak of 3.2 dB. Its PSD is shown in Fig. 3, together with that of the proposed precoder (order $\ell_0 = 1$) adjusted to yield the same spectral peak value. Although the N-continuous precoder achieves very low PSD values far away from the passband, the proposed design yields a much sharper PSD near the passband edges.

B. Symbol error rate

The impact of precoding at the receiver is illustrated now. Fig. 4 shows the SER attained with the DF-based decoder (14), and also with a reduced-complexity decoder which directly estimates the data as $\hat{\boldsymbol{d}}_m = \mathrm{DEC}\{\boldsymbol{G}_0^H \boldsymbol{r}_m\}$. Although this reduced-complexity decoder exhibits an error floor, it may be an attractive choice in low-distortion (i.e., small spectral peak) scenarios. On the other hand, the DF-based decoder successfully removes the inter-block interference introduced by the precoder. Although one may expect some SER degradation due to error propagation, we have only observed this effect for very large spectral peak values (not shown for brevity).

C. Effect of precoder order

For a memoryless precoder, the only way to improve performance is to increase redundancy, at the expense of sacrificing spectral efficiency. With the introduction of memory, this degradation can be ameliorated at the cost of additional computational complexity. To illustrate this fact, Fig. 5 shows the relative OBR as a function of memory precoder order ℓ_0, and for different redundancy values R, for 1-dB spectral peak.

[1]The memoryless precoder does not actually generate spectral peaks, but we show its OBR value for reference in Fig. 2.

$N_{\rm cp}$	$N/32$					$N/16$					$N/8$				
$R \setminus \ell_0$	0	1	2	3	4	0	1	2	3	4	0	1	2	3	4
2	-3.1	-8.7	-8.5	-7.8	-8.0	-2.6	-8.7	-8.3	-7.5	-7.8	-2.3	-8.7	-8.0	-7.5	-7.4
4	-9.8	-19.1	-20.3	-20.7	-21.2	-8.3	-18.5	-19.7	-19.3	-19.3	-7.2	-16.2	-17.5	-18.4	-18.9
6	-18.4	-30.9	-32.1	-32.6	-32.9	-16.7	-29.3	-29.4	-30.8	-32.2	-14.8	-26.0	-28.4	-29.2	-29.3
8	-26.1	-42.0	-43.6	-44.6	-45.7	-25.2	-40.6	-42.0	-43.7	-43.8	-23.4	-36.4	-40.6	-41.4	-43.2
10	-38.9	-55.7	-57.9	-59.0	-59.9	-33.4	-53.1	-55.8	-57.5	-58.6	-32.0	-50.2	-51.2	-51.7	-54.5

TABLE I
RELATIVE OBR (IN dB) OF MEMORY PRECODERS FOR DIFFERENT ORDERS, REDUNDANCIES, AND CP LENGTHS. $N = 256$, $K = 129$. SPECTRAL PEAK IS SET TO 1 dB IN ALL CASES.

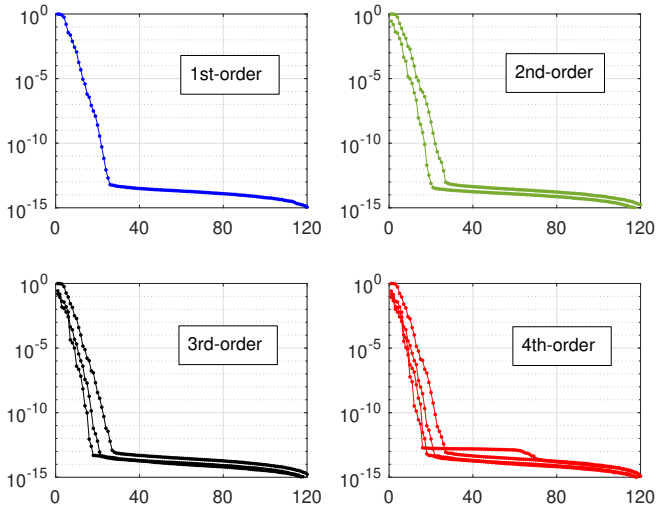

Fig. 6. Singular values of precoding matrices $\{\boldsymbol{G}_\ell,\, 1 \le \ell \le \ell_0\}$. $N = 256$, $N_{\rm cp} = N/4$, $K = 129$, $R = 8$. Spectral peak is set to 1 dB in all cases.

Clearly, for a given redundancy R, performance improves as the precoder order is increased; however, the performance gain eventually saturates, since the contribution of faraway symbols becomes less significant. The savings in spectral efficiency obtained with memory precoding can be seen in Fig. 5: for example, the performance of the memoryless precoder with $R = 10$ (efficiency $\frac{119}{129} = 92.25\%$) can be achieved with a fourth-order precoder and $R = 6$ (95.35%). This trend also holds for other CP lengths, as seen in table I.

Fig. 6 shows the singular values of the precoding matrices $\boldsymbol{G}_\ell$ for $\ell \ge 0$, for $R = 8$ and different precoder orders. It is clear that these matrices can be well approximated by low-rank ones, with the corresponding computational savings when performing the matrix-vactor products $\boldsymbol{G}_\ell \boldsymbol{d}_{m-\ell}$ at the transmitter, see (6), or $\boldsymbol{G}_\ell \hat{\boldsymbol{d}}_{m-\ell}$ at the receiver, as in (14).

VI. CONCLUSION

Orthogonal precoding is an appealing technique to reduce out-of-band radiation in multicarrier systems, but standard memoryless designs must pay a steep price in spectral efficiency. The introduction of memory in orthogonal precoding improves performance without sacrificing more spectrum at the cost of additional computational complexity. The proposed design allows to specify the frequency region of interest and to weight the influence of out-of-band emission.

REFERENCES

[1] 3GPP, "TS 38.211: NR; Physical channels and modulation (Release 15)," https://portal.3gpp.org/desktopmodules/Specifications/SpecificationDetails.aspx?specificationId=3213, Mar. 2018.

[2] M. Faulkner, "The effect of filtering on the performance of OFDM systems," *IEEE Trans. Veh. Technol.*, vol. 49, no. 5, pp. 1877–1884, 2000.

[3] X. Huang, J. A. Zhang, and Y. J. Guo, "Out-of-band emission reduction and a unified framework for precoded OFDM," *IEEE Commun. Mag.*, vol. 53, no. 6, pp. 151–159, Jun. 2015.

[4] M.-F. Tang and B. Su, "Joint window and filter optimization for new waveforms in multicarrier systems," *EURASIP J. Adv. Signal Process.*, vol. 2018, no. 1, pp. 63–82, Oct. 2018.

[5] K. Hussain and R. López-Valcarce, "Optimal window design for W-OFDM," in *IEEE Int. Conf. Acoust., Speech, Signal Process. (ICASSP)*, 2020, pp. 5275–5289.

[6] C.-D. Chung, "Spectrally precoded OFDM," *IEEE Trans. Commun.*, vol. 54, no. 12, pp. 2173–2185, Dec. 2006.

[7] J. van de Beek, "Sculpting the multicarrier spectrum: a novel projection precoder," *IEEE Commun. Lett.*, vol. 13, no. 12, pp. 881–883, Dec. 2009.

[8] R. Xu and M. Chen, "A precoding scheme for DFT-based OFDM to suppress sidelobes," *IEEE Commun. Lett.*, vol. 13, no. 10, pp. 776–778, Oct. 2009.

[9] M. Ma, X. Huang, B. Jiao, and Y. J. Guo, "Optimal orthogonal precoding for power leakage suppression in DFT-based systems," *IEEE Trans. Commun.*, vol. 59, no. 3, pp. 844–853, Mar. 2011.

[10] K. Hussain, A. Lojo, and R. López-Valcarce, "Flexible spectral precoding for sidelobe suppression in OFDM systems," in *IEEE Int. Conf. Acoust., Speech, Signal Process. (ICASSP)*, 2019, pp. 4789–4793.

[11] K. Hussain and R. López-Valcarce, "Memory tricks: Improving active interference cancellation for out-of-band power reduction in OFDM," in *Int. Workshop Signal Process. Adv. Wireless Commun. (SPAWC)*, 2021, pp. 86–90.

[12] J. van de Beek and F. Berggren, "N-continuous OFDM," *IEEE Commun. Lett.*, vol. 13, no. 1, pp. 1–3, Jan. 2009.

[13] M. Ohta, M. Okuno, and K. Yamashita, "Receiver iteration reduction of an N-continuous OFDM system with cancellation tones," in *IEEE Global Telecommun. Conf. (GLOBECOM)*, 2011, pp. 1–5.

[14] Y. Zheng, J. Zhong, M. Zhao, and Y. Cai, "A precoding scheme for N-continuous OFDM," *IEEE Commun. Lett.*, vol. 16, no. 12, pp. 1937–1940, Dec. 2012.

[15] L. Dan, C. Zhang, J. Yuan, P. Wen, and B. Fu, "Improved N-continuous OFDM using adaptive power allocation," in *IEEE Annu. Comput. Commun. Workshop and Conf. (CCWC)*, 2018, pp. 937–940.

[16] R. López-Valcarce, "General form of the power spectral density of multicarrier signals," *IEEE Commun. Lett.*, accepted.

[17] R. Kumar, K. Hussain, and R. López-Valcarce, "Mask-compliant orthogonal precoding for spectrally efficient OFDM," *IEEE Trans. Commun.*, vol. 69, no. 3, pp. 1990–2001, 2021.

[18] G. H. Golub and C. F. Van Loan, *Matrix Computations (3rd Ed.)*. Baltimore, MD, USA: Johns Hopkins University Press, 1996.

[19] I. V. L. Clarkson, "Orthogonal precoding for sidelobe suppression in DFT-based systems using block reflectors," in *IEEE Int. Conf. Acoust., Speech, Signal Process. (ICASSP)*, 2017, pp. 3709–3713.